Resistivity variation in heteroepitaxial $La_{0.7}Ca_{0.3}MnO_3/Gd_{0.67}Sr_{0.33}MnO_3$ multilayers with different thicknesses of the $La_{0.7}Ca_{0.3}MnO_3$ layers

1999 J. Phys.: Condens. Matter 11 3187

(http://iopscience.iop.org/0953-8984/11/15/024)

J. Phys.: Condens. Matter **11** (1999) 3187–3192. Printed in the UK PII: S0953-8984(99)97101-1

Resistivity variation in heteroepitaxial $La_{0.7}Ca_{0.3}MnO_3/Gd_{0.67}Sr_{0.33}MnO_3$ multilayers with different thicknesses of the $La_{0.7}Ca_{0.3}MnO_3$ layers

G C Xiong†, Z H Wang, G J Lian, D S Dai and Z Z Gan
Department of Physics, Peking University, 100871 Beijing, People's Republic of China

Received 28 August 1998, in final form 28 December 1998

Abstract. Resistivity measurements on $La_{0.7}Ca_{0.3}MnO_3/Gd_{0.76}Sr_{0.33}MnO_3$ (LCMO/GSMO) multilayers with different thicknesses of the LCMO layers are reported. The resistivity maximum temperature T_M indicates that the metal–insulator transition decreases with reducing LCMO layer thickness. Data above T_M show activated conduction behaviour with $\rho = CT\exp(E_a/k_BT)$, the temperature dependence of the conductivity for small-polaron hopping. The activation energy E_a increases with reducing LCMO layer thickness in the multilayers. The explanation of the properties of the LCMO/GSMO multilayers is twofold. For doped manganese oxides, these changes can be understood by (i) considering the effect of strain on the LCMO layers in the LCMO/GSMO multilayers and (ii) assuming that the ferromagnetic transition Curie temperature T_C and E_a depend on the Mn–O–Mn bond angle.

In recent years, there has been much attention paid to doped manganese oxides due to the discovery of magnetoresistance (MR) [1–5]. In $R_{1-x}A_xMnO_3$ (R = La, Nd, Pr and A = Ba, Sr, Ca, Pb), divalent substitution ($0.2 < x < 0.5$) results in a transition from a paramagnetic insulator to a ferromagnetic metal upon cooling, which is accompanied by a sharp resistivity peak. Applying an external magnetic field near the ferromagnetic transition Curie temperature T_C, a MR behaviour can be observed. The magnetic and electronic properties of the doped manganese oxides have been broadly explained by the double-exchange model [6]. Recently, theoretical and experimental studies have suggested that there is considerable coupling between the magnetism and the lattice in doped manganese oxide [7].

The ferromagnetic transition of $R_{1-x}A_xMnO_3$ depends on the doping level and oxygen concentration, which is attributed to the change of the Mn^{3+}/Mn^{4+} ratio [6]. Experiments have shown that T_C and the resistivity depend on the average radius of the A-site atom in $AMnO_3$ while the doping concentration remains constant; this is attributed to the changes in the Mn–O–Mn bond angle during the substitution of the A-site atom [1]. For example, $La_{0.7}Ca_{0.3}MnO_3$ (LCMO) is a ferromagnetic material at low temperature; however, no ferromagnetic transition is observed in $Gd_{0.76}Sr_{0.33}MnO_3$ (GSMO). Because LCMO and GSMO have similar structure, a heteroepitaxial structure can be achieved in the LCMO/GSMO multilayer system.

In the last decade, studies of magnetic metallic multilayers, such as Fe/Cr and Co/Cu alternating layers, and oxide high-temperature-superconducting superlattices, such as $YBa_2Cu_3O_7/PrBa_2Cu_3O_7$ [8], have attracted much attention. In the multilayers, there are

† E-mail address: ssxgc@pku.edu.cn.

0953-8984/99/153187+06$19.50

interfaces composed of two different materials, which provides a good opportunity to study the coupling, interaction, proximity and effects of strain etc across the interfaces of these materials. However, to date only a few studies on the manganese oxide multilayers have been performed [9]. In this paper, we present the temperature dependence of the electrical resistivity in LCMO/GSMO multilayers. LCMO/GSMO multilayers with different thicknesses of the LCMO layers were prepared by pulsed laser deposition (PLD). A standard four-probe method was used to measure the DC resistivities of the samples.

The PLD system and deposition process have been described previously [5]. Sintered ceramic targets with nominal compositions of $La_{0.7}Ca_{0.3}MnO_3$ and $Gd_{0.67}Sr_{0.33}MnO_3$ were used for preparing the LCMO/GSMO superlattices. Like in the fabrication of high-temperature-superconducting cuprate superlattices [8], the thicknesses of the LCMO and GSMO layers were controlled by adjusting the numbers of laser pulses. The thicknesses of single LCMO and GSMO thin films deposited by 3000 laser pulses were measured to calibrate the deposition rates of single laser pulses for the different targets. In the deposition of superlattices, the laser pulses were controlled by a computer and the targets were changed *in situ* as required. The superlattices were grown at the substrate temperature of $T_S = 750\ ^\circ C$ on (100)-oriented $LaAlO_3$ single-crystal substrates with 50 nm GSMO buffer layers. During deposition, the oxygen partial pressure was kept at 25 Pa. After deposition, the as-grown films were directly cooled down to room temperature in O_2. Under these deposition conditions, x-ray diffraction θ–2θ patterns for as-grown samples in the range 20°–50° only show (002) and (004) peaks besides the substrate reflections, which indicates the growth orientation. Further confirmation of the heteroepitaxial growth has been obtained from high-resolution transmission electron microscopy investigations of the films.

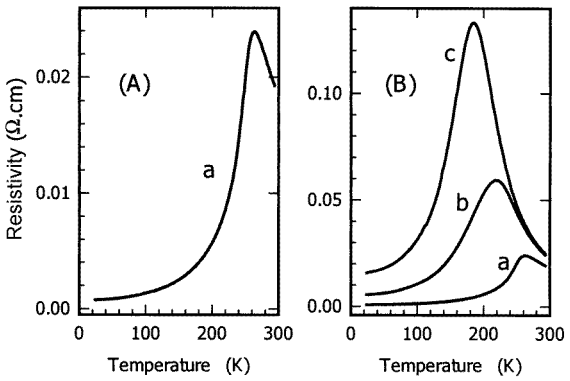

Figure 1. Resistivity versus temperature curves in zero field for (a) epitaxial LCMO film and multilayers of (b) [LCMO(18.6 nm)/GSMO(6.2 nm)]$_4$ and (c) [LCMO(12.4 nm)/GSMO(6.2 nm)]$_4$.

In resistivity versus temperature (ρ–T) measurements, the samples show resistivity maxima at a temperature T_M with MR behaviour. Curve (a) in figure 1 shows the ρ–T curve of a 150 nm LCMO film. A ferromagnetic transition is observed in the magnetization measurement for the LCMO film. In the ρ–T curve of the epitaxial LCMO film, a resistivity maximum of 24 mΩ cm is observed at $T_M = 262$ K. Below 260 K the electric resistivity drop is quite sharp, which indicates the ferromagnetic transition in the film. The resistivity maximum of the epitaxial film occurs at about the same temperature as for bulk LCMO samples. In applied magnetic fields, a MR behaviour is observed. The resistivities of this epitaxial LCMO film at room temperature and 100 K are 19 mΩ cm and 1.3 mΩ cm, respectively. The ρ–T curve of

GSMO film exhibits semiconductor behaviour with much higher resistivity; therefore for the LCMO/GSMO multilayers only the resistivity of the LCMO layers is calculated.

In multilayers, the resistivity of the LCMO layers at room temperature slightly increases and a similar resistivity peak feature is observed. Curves (b) and (c) in figure 1 show ρ–T in zero field for multilayers of (b) [LCMO(18.6 nm)/GSMO(6.2 nm)]$_4$ and (c) [LCMO(12.4 nm)/GSMO(6.2 nm)]$_4$, where the numbers represent the thicknesses of the layers and the multilayer period respectively. On reducing the thicknesses of the LCMO layers to 18.6 and 12.4 nm, the resistivity maximum temperatures decrease to $T_M = 218$ K and 185 K respectively; meanwhile, the resistivities increase substantially as observed in figure 1. Using the lattice constant of $c = 0.775$ nm for the bulk target, the thicknesses of the LCMO layers are about 24 and 16 unit cells, respectively. Figure 2 shows the ρ–T curves of multilayers in zero field and magnetic fields of 1, 3 and 5 T for (A) [LCMO(18.6 nm)/GSMO(6.2 nm)]$_4$ and (B) [LCMO(12.4 nm)/GSMO(6.2 nm)]$_4$. As observed for LCMO films, the LCMO/GSMO multilayers also demonstrate a typical MR behaviour; the resistivity is suppressed and T_M is increased as B is raised.

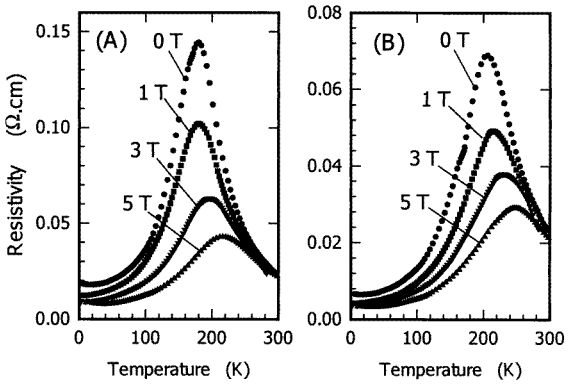

Figure 2. ρ–T curves of multilayers for (A) [LCMO(18.6 nm)/GSMO(6.2 nm)]$_4$ and (B) [LCMO(12.4 nm)/GSMO(6.2 nm)]$_4$ in zero field and magnetic fields of 1, 3, 5 T.

There are several parameters which could affect the resistivity of the multilayers. In order to separate the effects, two kinds of multilayer have been fabricated by changing the non-ferromagnetic target $Gd_{0.67}Sr_{0.33}MnO_3$ to $Gd_{0.7}Ca_{0.3}MnO_3$ and varying the thickness of GSMO from 6.2 to 9.3 nm. These changes do not introduce distinctive differences in resistivity behaviour. These results and figure 1 clearly demonstrate that the changes of the resistivity and T_M for the multilayers stem from the multilayer structure.

More samples are used to distinguish the variations in the resistivity and T_M. Figure 3 shows ρ–T curves for the LCMO monolayer sample and the multilayer samples with LCMO layer thicknesses of 24.8, 18.6, 12.4, 9.3, 6.2 nm and a thickness of GSMO of 6.2 nm. Clear tendencies of increasing resistivity and decreasing T_M with reducing LCMO layer thickness in the LCMO/GSMO multilayers can be recognized in figure 3. Upon reducing the thickness of the LCMO layers from 24.8 to 9.3 nm, the resistivity maximum temperatures monotonically decrease from $T_M = 234$ K to 89 K.

The resistivity maximum temperature T_M indicates the metal–insulator transition of the films, which is associated with the ferromagnetic ordering temperature T_c of the samples. Several different models have been suggested to explain the conduction mechanism above T_M. Each predicts a different temperature dependence of the resistivity. Variable-range hopping

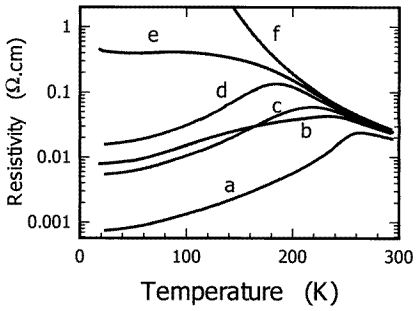

Figure 3. ρ–T curves for (a) the epitaxial LCMO film and LCMO/GSMO multilayers with a thickness of GSMO of 6.2 nm and LCMO layer thicknesses of (b) 24.8, (c) 18.6, (d) 12.4, (e) 9.3, (f) 6.2 nm.

has been suggested with the formula $\rho = C\exp(T_0/T)^{1/4}$ used to explain the resistivity behaviour [10]. Other authors have invoked the semiconductor formula $\rho = C\exp(E_g/k_BT)$, where E_g represents a band gap [11]. In the small-polaron-hopping model the polaron can be thought of as trapped inside a local energy well of height E_a, i.e., the activation energy of hopping [12, 13]. In the adiabatic approximation, the polaron is assumed to lead to $\rho = CT\exp(E_a/k_BT)$ [14]. According to Emin and Holstein, $C = 2k_B/3ne^2a^2\nu$. Here k_B is the Boltzmann constant, e is the electronic charge, n is the number density of the charge carriers, a is the site-to-site hopping distance and ν is the frequency of the longitudinal optical phonon that carries the polaron through the lattice. For our multilayer samples, the variable-range-hopping model gives a better curve fit. When the resistivity of the multilayers is replotted in the form $\ln(\rho/T)$–$1/T$ as in figure 4, an approximately linear behaviour above T_M can be recognized, which illustrates the law $\rho = CT\exp(E_a/k_BT)$.

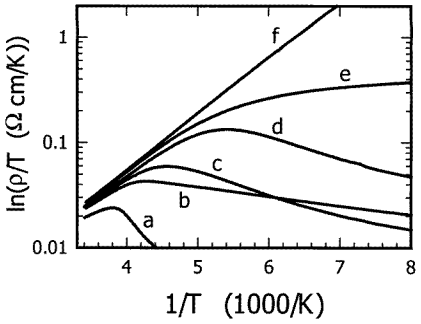

Figure 4. $\ln(\rho/T)$–$1/T$ curves for the temperature range from 300 to 125 K for (a) the epitaxial LCMO film and LCMO/GSMO multilayers with a thickness of GSMO of 6.2 nm and LCMO layer thicknesses of (b) 24.8, (c) 18.6, (d) 12.4, (e) 9.3, (f) 6.2 nm.

It is known that an oxygen deficiency results in a decreasing of T_c. In our experiment all of the samples were deposited under the same conditions and should have the same oxygen content. Some of the multilayer samples were annealed in a furnace at 900 °C for 0.5 h, which did not cause any change in the ρ–T curves. This annealing experiment indicates that the local disorder is not the reason for the variation of the resistivity and T_c. It is interesting that E_a increases with reducing LCMO layer thickness as can be seen in figure 4. There are several possible mechanisms that can affect the transport properties of LCMO/GSMO multilayers.

Recent experiments have shown that T_c depends on the Mn–O–Mn bond angle, as determined by controlling the average radius of the A-site atom in $AMnO_3$ while keeping the doping concentration constant [1]. If one considers the effect of strain on the LCMO layers in the LCMO/GSMO multilayers, the results can be understood on the basis of the assumption that T_c and E_a depend on the Mn–O–Mn bond angle. This assumption is reasonable, since T_c depends on the magnetic coupling between ions, and a distorted Mn–O–Mn bond angle leads to a weakness of the magnetic coupling. The radii of the Pr atom and the Y atom are smaller than that of the La atom, which leads to a distorted Mn–O–Mn bond angle and lower T_c for the $(La_{1-x}Pr_x)_{0.7}Ca_{0.3}MnO_3$ and $(La_{1-x}Y_x)_{0.7}Ca_{0.3}MnO_3$ systems [1]. It has been found that the strain caused by lattice mismatch between substrates and films can have an effect on the electrical transport properties and magnetoresistance in epitaxial doped manganese oxide thin films [15]. In the LCMO/GSMO multilayers, strain exists because of the difference in radii of the Gd atom and the La atom. On reducing the thickness of the LCMO layers, the effective strain will increase and lead to a lower T_c. Furthermore, since a distorted Mn–O–Mn bond angle means a higher energy barrier for the polaron to hop over, one may expect the effective strain on the LCMO layers to contribute to higher activation energies in the resistivity behaviour, as observed in figure 4. In the interface region of the LCMO/GSMO multilayers, it is possible that the number of effective carriers decreases. This could result in increases of the resistivity and resistivity coefficient C with reducing thickness of the LCMO layers.

Very recently, experimental results have demonstrated that the electrical transport properties of thin films are different from those of bulk materials [16]. Wang and Li reported a strain-induced large low-field MR in $Pr_{0.67}Sr_{0.33}MnO_3$ ultrathin films [15]. They suggested that the large low-field MR is due to strain-induced magnetic anisotropy and spin-dependent scattering at domain boundaries. A large low-field MR has also been obtained in LCMO/$Gd_{0.7}Ca_{0.3}MnO_3$ superlattices [9]. The transport properties and MR behaviour observed for the doped manganese oxide multilayers are similar to those observed for ultrathin films, which implies that strains and the spin-dependent scattering may play an important role in these materials.

In the doped manganese oxide multilayers, there is a big difference in conductivity across the ferromagnetic–paramagnetic interface. Besides the electrical transport properties, there is magnetic coupling between the ferromagnetic LCMO layers. The variation of the magnetic coupling via the spacer layers in the LCMO/GSMO multilayers should be considered also in explanations.

In conclusion, LCMO/GSMO multilayers show that the resistivity maximum temperature T_M decreases and the activation energy E_a increases with reducing thickness of the LCMO layers. The explanation of the properties of the LCMO/GSMO multilayers is twofold. For the doped manganese oxides, these results can be understood (i) on the basis of the assumption that T_c and E_a depend on the Mn–O–Mn bond angle and (ii) by considering the effect of strain on the LCMO layers in the LCMO/GSMO multilayers.

Acknowledgment

This work was partly supported by the National Natural Science Foundation of China (19674001).

References

[1] Hwang H Y, Cheong S-W, Radaelli P G, Mareezio M and Batlogg B 1995 *Phys. Rev. Lett.* **75** 914
[2] Satpathy S, Popovic Z S and Vukajlovic F R 1996 *Phys. Rev. Lett.* **76** 960

[3] Billinge S J L, DiFrancesco R G, Kwei G H, Neumeier J J and Thompson J D 1996 *Phys. Rev. Lett.* **77** 715
[4] Booth C H, Bridges F F, Kwei G H, Lawrence J M, Cornelius A L and Neumeier J J 1998 *Phys. Rev. Lett.* **80** 853
[5] Xiong G C, Zhang B, Wu S C, Lui Z X, Lian G J and Dai D S 1996 *Solid State Commun.* **97** 17
[6] van Santen J H and Jonker G H 1950 *Physica* **16** 599
Jonker G H 1956 *Physica* **22** 707
Zener C 1951 *Phys. Rev.* **82** 403
de Gennes P G 1960 *Phys. Rev.* **118** 141
[7] Millis A J, Littlewood P B and Shraiman B I 1995 *Phys. Rev. Lett.* **74** 5144
Asamitsu A, Moritomo Y, Tomioka Y, Arima T and Tokura Y 1995 *Nature* **373** 407
[8] Bozovic I and Eckstein J N 1996 *Physical Properties of High Temperature Superconductors* vol 5, ed D M Ginsberg (Singapore: World Scientific) p 99 and references therein
[9] Lian G J, Wang Z H, Gao J, Kang J F, Li M Y and Xiong G C 1999 *J. Phys. D: Appl. Phys.* **32** 90
[10] von Helmolt R, Wecker J, Samwer K, Haupt L and Barner K 1994 *J. Appl. Phys.* **76** 6925
[11] Jaime M, Salamon M B, Pettit K, Rubinstein M, Treece R E, Horwitz J S and Chrisey D B 1996 *Appl. Phys. Lett.* **68** 1576
[12] Ohtaki M, Koga H, Tokunaga T, Eguchi K and Arai H 1995 *J. Solid State Chem.* **120** 105
[13] Worledge D C, Snyder G J, Beasley M R and Geballe T H 1996 *J. Appl. Phys.* **80** 5158
Worledge D C, Mieville L and Geballe T H 1998 *Phys. Rev.* B **57** 15 267
[14] Emin D and Holstein T 1969 *Ann. Phys.* **53** 439
[15] Wang H S and Li Qi 1998 *Appl. Phys. Lett.* **73** 2360 and references therein
[16] Li X W, Gupta A, Xiao Gang and Gong G Q 1998 *J. Appl. Phys.* **83** 7049 and references therein